ACADEMIC PRESS

Available online at www.sciencedirect.com

SCIENCE DIRECT®

Icarus 162 (2003) 59–73

ICARUS

www.elsevier.com/locate/icarus

The structure, ordering and equation of state of ammonia dihydrate ($NH_3 \cdot 2H_2O$)

A.D. Fortes,* I.G. Wood, J.P. Brodholt, and L. Vočadlo

Research School of Geological and Geophysical Sciences, Birkbeck College and University College London, Gower Street, London WCIE 6BT, UK

Received 13 March 2002; revised 20 August 2002

Abstract

We present the first ab initio simulations of the low-pressure phase of ammonia dihydrate ($NH_3 \cdot 2H_2O$), ADH I, a likely constituent of many volatile-rich solid bodies in the outer Solar System (e.g., Saturn's moons). Ordered monoclinic (space group $P2_1$) and orthorhombic (space group $P2_12_12_1$) variants of the experimentally observed cubic cell (space group $P2_13$) may be constructed, with fully ordered water molecule orientations that obey the ice rules. Our calculations show that the most stable structure at 0 K is orthorhombic ($P2_12_12_1$), the monoclinic variants ($P2_1$) being energetically disfavored. We provisionally call this ordered orthorhombic phase ADH III. The, as-yet-unmeasured, bulk modulus, K_0, is predicted to be $10.67^{+0.56}_{-0.44}$ GPa at 0 K. Our results are also combined with literature data to arrive at a revised coefficient of volume thermal expansion, $\alpha_v = 2.81 \times 10^{-7}\, T^{1.39}$ (from 0–176 K), with the density at 0 K, $\rho_0 = 991.7(39)$ kg m^{-3}. We also present a case, based on literature data, that argues for a gradual transformation from a paraelectrically disordered cubic structure ($P2_13$) to the proposed antiferroelectrically ordered orthorhombic structure ($P2_12_12_1$) around 130–150 K (cf. ice III ↔ IX), a temperature regime that applies to the surfaces and interiors of many medium-sized (radii ~500–700 km) icy bodies.

Keywords: Ices; Interiors; Mineralogy; Satellites of Saturn; Satellites of Uranus

I. Introduction

Of the "rock-forming" minerals expected to compose the mantles of icy moons in the outer Solar System, ammonia dihydrate (ADH), $NH_3 \cdot 2H_2O$, is perhaps one of the least well understood.

Models of planetary accretion (e.g., Lewis, 1972; Prinn and Fegley, 1981) and photogeological observations of cryovolcanic landforms (e.g., Kargel, 1992), combined with isotopic studies of the Titan's volatile reservoir (Lunine et al., 1999), indicate that the condensed volatile mineral (CVM) component of icy moons orbiting Saturn, Uranus, and Neptune contains ~5–15 wt% NH_3. Consideration of the ambient pressure phase diagram (Kargel, 1992) for the system H_2O–NH_3 reveals, therefore, that ADH will be an important mineral species in outer Solar System moons.

Ammonia has a dramatic effect on the melting behavior of ice, and analogies have been drawn between the melting behavior under pressure and the more familiar MgO–SiO_2 system (Hogenboom et al., 1997), with all the attendant implications for the eruption of cryovolcanic liquids (e.g., Stevenson, 1982; Johnson and Nicol, 1987; Kargel, 1992; Yarger et al., 1993). It has also been proposed that Saturn's largest moon, Titan, may still retain a deep ocean, or aquasphere, of eutectic ammonia–water fluid beneath a crust of water ice (Grasset and Sotin, 1996; Grasset et al., 2000), and this has been recognized as a site of potential interest to exobiologists (Fortes, 2000). The crystallization of ammonia hydrates has also been advocated as the mechanism for generating global expansion and rifting on moons such as Tethys and Rhea (Consolmagno, 1985).

The ammonia hydrates in general are also of broader interest, from the point of view of chemical physics, since they are the simplest system to contain mixed (heteronuclear, O–H. . .N, and homonuclear, O–H. . .O) hydrogen bonds of the kind common in many more complex biomolecules.

* Corresponding author. Fax: +44-0-20-7387-1612.
E-mail address: andrew.fortes@ucl.ac.uk (A.D. Fortes).

0019-1035/03/$ – see front matter © 2003 Elsevier Science (USA). All rights reserved.
doi:10.1016/S0019-1035(02)00073-8

Table 1
Structural parameters for the cubic disordered unit cell of ADH I (Loveday and Nelmes, 2000) at zero pressure, 150 K

Space group $P2_13$

a (Å) 7.1272(8)
V (Å^3) 362.04(12)

Fractional atomic coordinates

	Wyckoff position	Occupancy	x	y	z
O1	4*a*	1	0.69702 (30)	0.69702 (30)	0.69702 (30)
H1	12*b*	2/3	0.75253 (51)	0.67696 (54)	0.57222 (58)
O2	4*a*	1	0.15812 (35)	0.15812 (35)	0.15812 (35)
H2	12*b*	1	0.23785 (33)	0.23785 (33)	0.23785 (33)
H3	12*b*	1/3	0.0282 (14)	0.21182 (99)	0.17317 (107)
N1	4*a*	1	0.38105 (30)	0.38105 (30)	0.38105 (30)
H4	12*b*	1	0.35783 (34)	0.35963 (35)	0.51403 (55)

Bond lengths (Å)

O1–H1	0.984 (5)	H1. . .O2	1.766 (5)
O2–H2	0.984 (3)	H2. . .N1	1.768 (3)
O2–H3	1.008 (10)	H3. . .O1	1.74 (1)
N1–H4	0.974 (5)	H4. . .O1	2.395 (5)
O1. . .O2	2.747 (3)	O2. . .N1	2.752 (3)

We are interested, therefore, in understanding the phase relations and physical characteristics of polymorphs across the whole ammonia–water system. Our research program employs ab initio simulation as the principal means of achieving this goal, and results for ammonia monohydrate (AMH) are reported elsewhere (Fortes et al., 2001). We present here the results of our initial investigation on the low-pressure phase of ADH (ADH I). In Section II we commence with a description of the time- and space-averaged structure of ADH I as obtained from X-ray and neutron diffraction experiments. We will then describe the rules governing the orientation of water molecules within this structure, and hence derive a set of ordered and disordered cells that reflect the instantaneous local structure of ADH I. This is followed in Section III by an account of the computational method employed in the simulation of these cells, and Section IV describes our results. The results include a comparison of the total energies of the ordered structures and the fitting of an equation of state (EOS) to the calculated energy of the ordered cells as a function of molar volume. In Section V we will discuss the implications of our results for the structure and ordering of ADH I throughout its pressure–temperature stability field (0–176.16 K, 0–0.5 GPa), and compare our predictions with the available experimental evidence. In Section VI we will outline some of the potential implications of this work in understanding the surfaces and interiors of icy planetary bodies.

II. Structures

The structure of ADH I observed in X-ray diffraction (Bertie and Shehata 1984) and neutron diffraction (Loveday and Nelmes, 2000) experiments is cubic, space group $P2_13$ (with $Z = 4$). The threefold site symmetry of the water molecule rules out an ordered structure under this space group, and so the water molecules in ADH I must be orientationally disordered. This disorder is represented crystallographically by partially occupied hydrogen sites. The lattice parameters and internal coordinates of the disordered cubic structure are presented in Table 1. ADH I transforms into a denser polymorph, ADH II, of unknown structure at 0.3–0.5 GPa (Hogenboom et al., 1997; Loveday et al., 1999). The phase relations are shown in Fig. 11.

The zeolite-like heavy atom structure of ADH I (Fig. 1) is dominated by a strongly hydrogen-bonded framework of water molecules that has broad channels along the *a*, *b*, and *c* axes. Ammonia molecules are sited in these channels. The ice framework consists of two types of oxygen site (Fig. 2). The first, O1, is hydrogen bonded to three neighboring O2 sites. There are three hydrogen sites (H1) around each O1, over which the two hydrogen atoms covalently bound to O1 are disordered. Thus, these hydrogen sites are 2/3 occupied. The oxygen atoms on the O2 sites are hydrogen bonded to three O1 atoms and to one ammonia molecule. Four hydrogen sites surround O2. The site along the O–N vector (H2) is always occupied. The remaining hydrogen atom is then disordered over the other three possible sites. Hence, these sites (H3) are 1/3 occupied.

However, this picture only describes the time- and space-averaged structure of ADH I. On a local scale, we expect that the molecular orientations will obey the ice rules proposed by Bernal and Fowler (1933). These rules stipulate the following:

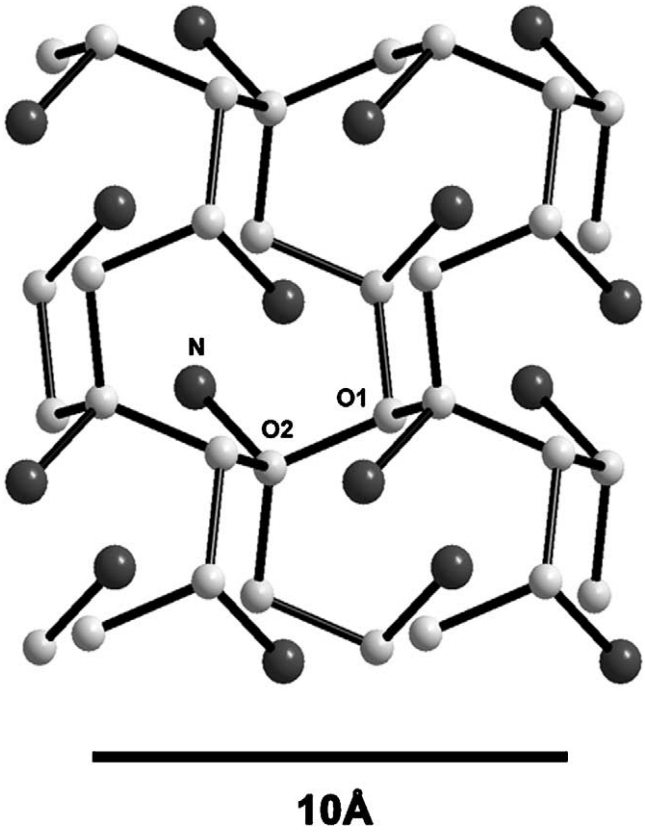

Fig. 1. The heavy atom framework in ADH I viewed down the *a* axis. Light gray spheres are oxygen atoms. Dark gray spheres are nitrogen atoms. The structure bears a superficial similarity to the APC zeolite topology.

1. Each oxygen atom is bound to two hydrogen atoms by covalent O–H bonds approximately 0.97 Å long. In other words, water molecules are preserved in the solid state as distinct structural units.
2. These hydrogen atoms lie more or less along the vectors between neighboring oxygen atoms, but there can only be one such hydrogen atom between a given pair of oxygen atoms.

Thermally activated reorientation of the water molecule (and hence ordering) can only occur if the ice rules are broken, which in turn requires point defects in the structure (e.g., Gränicher, 1958). The first rule is broken at ionic defects. These are the result of proton transfer along a hydrogen bond, yielding neighboring H_3O^+ and OH^- ions (Fig. 3a). The second rule is broken at rotational defects, known as Bjerrum defects; these are of two varieties (Fig. 3b): L-type defects, in which there are no hydrogen atoms between neighboring oxygen atoms, and D-type defects where there are two hydrogen atoms between neighboring oxygen atoms (Bjerrum, 1951, 1952). These cartoons show the same section of crankshaft chain as appears in Fig. 2. Although molecular dynamics simulations (Podeszwa and Buch, 1999) reveal the nature of orientational defects to be rather more complex, we will hold to the simple picture presented by Bjerrum (1951, 1952).

We expect that the instantaneous local structure in the dynamically disordered ADH I cell will be as depicted in Fig. 3c, which obeys the ice rules and which lowers the local symmetry from cubic. This explains the observation of a splitting in the $\nu_3(NH_3)$ branch in the infrared spectrum that is forbidden under cubic symmetry (Bertie and Shehata 1984). Infrared spectroscopy samples length scales on the order of a few unit cells, and will therefore "sense" the lower local symmetry of an ADH structure that is constrained by the ice rules. There will be some temperature-dependent density of ionic defects and Bjerrum defects in the structure. These allow for reorientation and thus for the exhibition of disorder over greater temporal and spatial scales. Neutron diffraction, for example, samples length scales of order 10^3 Å (based on the width of the observed Bragg peaks).

Since no experimental evidence for superlattices in ADH has been reported, we confine our discussion here to unit cells that are dimensionally equivalent to the disordered cubic cell. Working with this cell and applying the constraints of the ice rules we find that there are only nine possible unit cells (variants A to I: Fig. 4), which differ in the orientation of their water molecules. Six of these nine cells (variants A to F) retain only a single 2_1-rotation axis (i.e., they belong to the monoclinic symmetry class 2), while the remaining three cells (variants G, H, and I) possess three

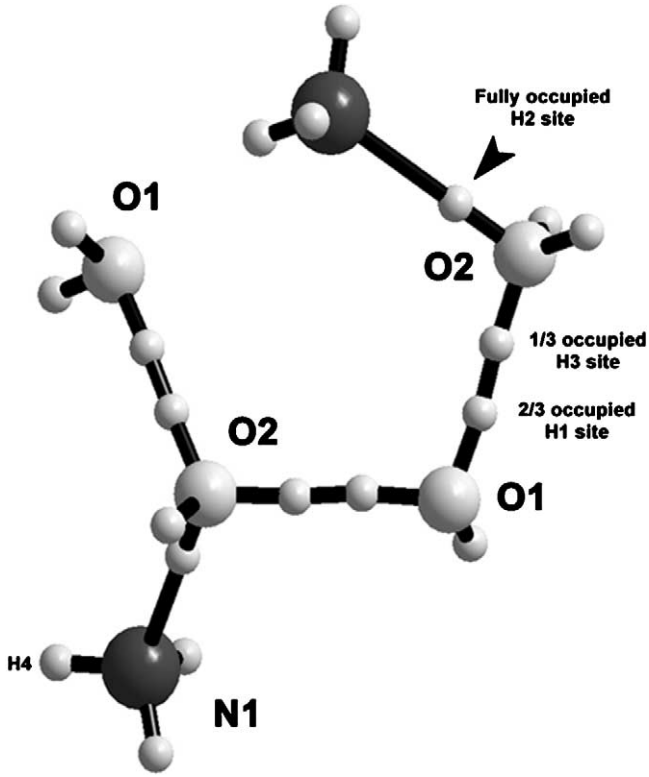

Fig. 2. The arrangement of partially occupied hydrogen sites along a section of hydrogen-bonded crankshaft in ADH I. The designation of the atoms in the asymmetric unit refers to the atomic labels in Table 1.

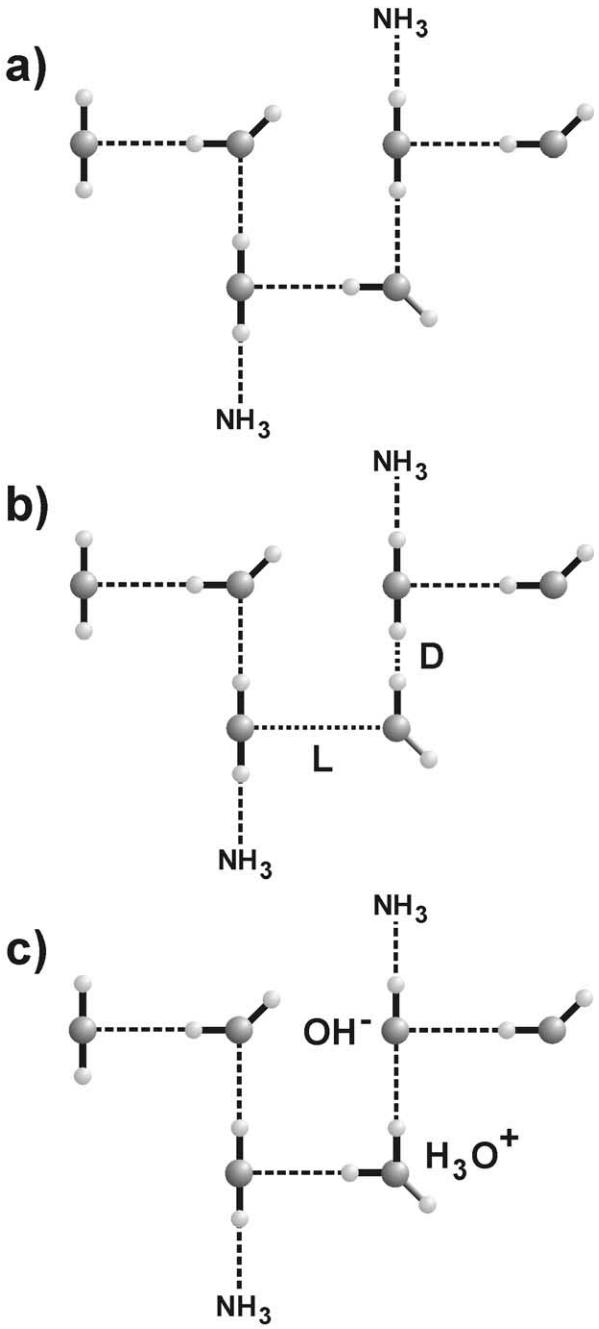

Fig. 3. (a) Cartoon representation of the crankshaft depicted in Fig. 2 after the introduction of an ionic defect (H_3O^+ and OH^-), thus breaking the ice rules. (b) As above but with a Bjerrum defect pair (L and D, described in the text) introduced. (c) A neatly ordered arrangement of water molecules, obeying the ice rules.

orthogonal 2_1 axes (orthorhombic class 222), losing only the triad axes of the cubic cell (class 23).

Breaking the ice rules (i.e., by introducing point defects) typically reduces the symmetry of the cell to triclinic, although there are some very unlikely configurations (e.g., with all of the O1 atoms as H_3O^+ and all of the O2 atoms as OH^-), which preserve the symmetry elements of cubic class 23.

The six monoclinic cells all turn out to be identical to one another, as do the three orthorhombic cells. If, for example, we take the first cell in Fig. 4 (variant A), look down the *b* axis, instead of looking down the *a* axis, and make a rotation of 90° clockwise (exactly equivalent to a 120° rotation around the missing threefold axis) we would see an arrangement that is identical to variant B. A further 120° rotation about the missing threefold axis yields variant C, and performing the operation of the absent 2_1 axes then yields variants D to F. The same is true of the three orthorhombic cells, which are related to one another by the missing threefold axis of the parent cubic cell. There are then, not nine, but only two unique arrangements of the hydrogen atoms in ADH I that satisfy the ice rules. In the monoclinic cell the ordering is rather untidy (the distance between the hydrogen atoms of neighboring water molecules is not maximized) and the dipole moments of the water molecules do not cancel out, leaving a moment of $\sim 6.7 \times 10^{-30}$ Cm per formula unit along the 2_1-axis, i.e., the crystal is ferroelectric. In the orthorhombic cell the ordering is much neater, maximizing the distance between the hydrogen atoms of neighboring water molecules, and the water molecules are arranged such that their dipole moments cancel each other out, giving an antiferroelectric crystal.

It is important to note that the ordered variants can twin, *while preserving the ice rules*, on a number of planes (e.g., on the (100), or (020) planes), although the number of permutations is larger for the orthorhombic variants by virtue of the higher symmetry. The twinning operations correspond to the lost threefold axes of the cubic space group; the effect of such twinning will be to produce a composite crystal that might contain, for example, all three of the orthorhombic orientational variants shown in Fig. 4G–I.

In Section IV we will report the results of ab initio simulations on the two cells that obey the ice rules, but we first describe the computational method used.

III. Computational method

The ab initio pseudopotential method, based on density functional theory (Hohenberg and Kohn, 1964; Kohn and Sham, 1965), was used for calculating the total energy of the crystal. The Perdew–Wang generalized gradient corrected functional (PW91) was used to represent the exchange-correlation potential (Perdew and Wang, 1992), this form of the generalized gradient approximation (GGA) having been demonstrated to yield the most accurate results in hydrogen-bonded systems (Hamann, 1997; Tsuzuki and Lüthi, 2001). Core electrons are replaced by Vanderbilt non-normconserving ultrasoft pseudopotentials (Vanderbilt, 1990), themselves formulated within the GGA, and the valence electron wavefunctions are expanded as a plane-wave basis set. Total energy calculations were performed using the VASP (Vienna *Ab Initio* simulation Package) code

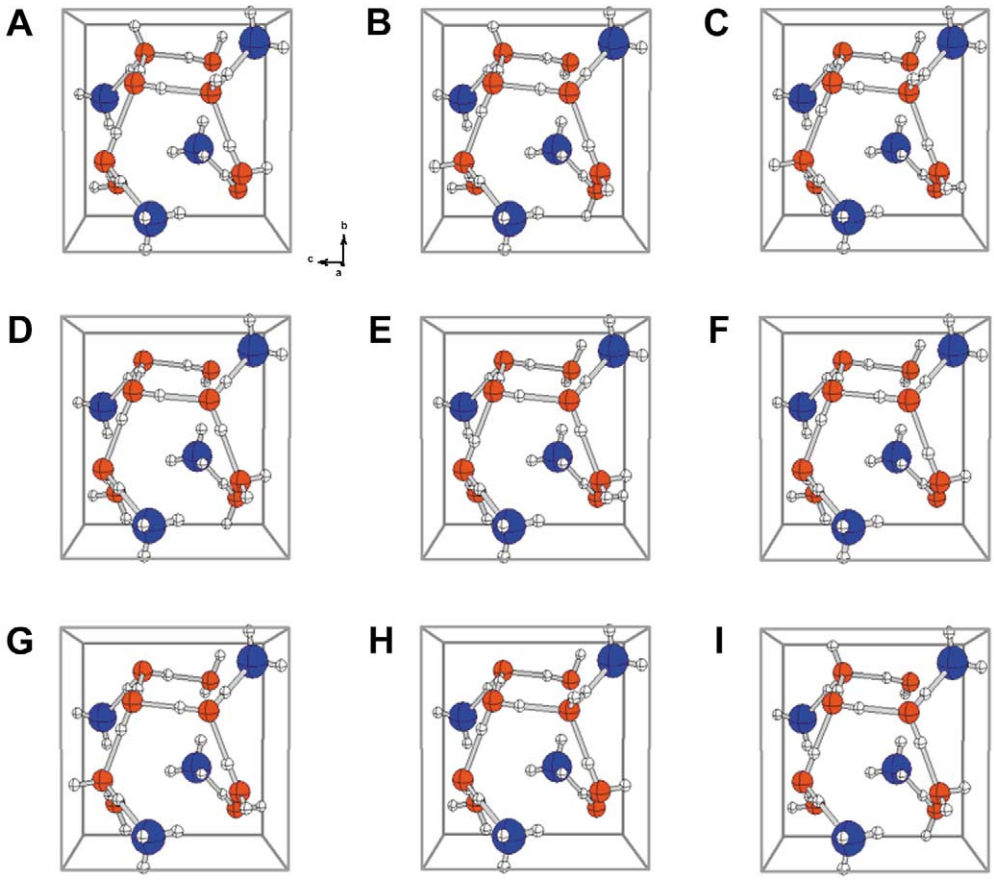

Fig. 4. Variants A to I are the nine possible permutations of the water molecules in the ADH unit cell allowed by the ice rules. Variants A to F have only a single 2_1 rotation axis. Variants G, H, and I have three orthogonal 2_1 axes.

(Kresse and Furthmüller, 1996). Total energy convergence tests were carried out to optimize the sampling of the Brillouin zone, and the cutoff of the plane-wave basis set. The Monkhorst–Pack scheme (Monkhorst and Pack, 1976) was used for sampling of the Brillouin zone and it was found that a 4×4×4 grid of $\bar{k}$ -points, combined with a kinetic energy cutoff of 1100 eV, yielded total energy convergence to better than 10^{-4} eV per unit cell. A series of fixed volume calculations were then performed in which the ions were allowed to move according to the calculated Hellman–Feynman forces. For each volume specified the structure was relaxed in order to optimize the lattice parameters and internal coordinates.

As a test of the reliability of the supplied pseudopotentials the relaxed geometry of isolated monomers of both water and ammonia was calculated. For the isolated water molecule we found the O–H bond length, $r_{(O–H)} = 0.970$ Å, and the bond angle, H–Ô–H = 104.74°. These values compare well with the experimental values of 0.95785 Å and 104.5424° (Jensen 1989). For the isolated ammonia molecule we found the N–H bond length, $r_{(N–H)} = 1.022$ Å, and the bond angle H–N̂–H = 107.29°. Again, these are a good match to the experimental values, 1.011 Å and 106.80° (Demaison et al., 2000). The error of 1–1.5% in the length of the X–H bond is largely due to inadequacies in the hydrogen pseudopotential. In principle, this can be corrected by a slight increase in the strength of the nonlocal part of the pseudopotential (Andrews et al., 1997).

While the PW91 functional we have used does not properly account for dispersion forces, it has been found to be superior to other GGA functionals (e.g., Tsuzuki and Lüthi, 2001), yielding very good results in solids dominated by O–H. . .O hydrogen bonds, and we have confirmed its performance in previous work on AMH (Fortes et al., 2001).

IV. Results

A. Equation of state

Structural relaxations were carried out on both the monoclinic and orthorhombic cells at a series of fixed volumes over which, based on our experience with ammonia monohydrate (Fortes et al., 2001), we expected ADH to remain molecular, that is, 42–56 $cm^3\ mol^{-1}$ (approximately −1 to 5 GPa). Our earlier work had indicated a propensity toward proton transfer from O to N at pressures of ∼5 GPa, yielding ammonium hydroxide hydrate. The relaxed cell dimensions and fractional atomic coordinates of the proposed ordered orthorhombic and monoclinic cells (with the

Table 2
Structural parameters for the ordered orthorhombic unit cell of ADH I (variant G), derived from the disordered cubic cell (as described in Section II) and relaxed (as described in Section III)

Space group $P2_12_12_1$

a (Å) 7.1604
b (Å) 7.0639
c (Å) 7.1577
V (Å^3) 362.04

Fractional atomic coordinates

	Wyckoff position	Occupancy	*x*	*y*	*z*
O1	4*a*	1	0.6562	0.3397	0.8469
H1	4*a*	1	0.2587	0.7562	0.7359
H2	4*a*	1	0.7919	0.6680	0.4764
O2	4*a*	1	0.6936	0.6939	0.7016
H3	4*a*	1	0.9351	0.2542	0.1786
H4	4*a*	1	0.6749	0.5637	0.7551
N1	4*a*	1	0.6258	0.8727	0.1258
H5	4*a*	1	0.1541	0.4860	0.8600
H6	4*a*	1	0.5121	0.3518	0.3427
H7	4*a*	1	0.8540	0.1642	0.4887

Bond lengths (Å)

O1–H1	1.035	H1. . .N1	1.647
O1–H2	1.000	H2. . .O2	1.786
O2–H3	1.005	H3. . .O1	1.726
O2–H4	1.005	H4. . .O1	1.719
N1–H5	1.024	H5. . .O2	2.375
N1–H6	1.023	H6. . .O2	2.359
N1–H7	1.026	H7. . .O2	2.312
O1. . .N1	2.682	O2–H3. . .O1	2.730
O2. . .H2–O1	2.767	O2–H4. . .O1	2.723

volume constrained to be the same as for the neutron-derived cubic cell) are given in Tables 2 and 3, respectively.

The first point of note is that the energies of the monoclinic and orthorhombic cells are not the same (see Fig. 5 and Table 4). At zero pressure, there is an extremely small energy difference of 5 meV per formula unit (~0.5 kJ mol^{-1}), with the antiferroelectrically ordered orthorhombic cell being the more energetically favorable. Therefore, all else being equal, the water molecules in ADH I will prefer any one of the three energetically degenerate variants G, H, or I (Fig. 4). We wished to discover whether the monoclinic cell was stabilized relative to the orthorhombic cell under pressure, but the energy–volume, $E(V)$, data (Fig. 5) show that that the monoclinic cell is energetically disfavored under all compressions simulated.

Integrated forms of the Birch–Murnaghan equation of state (Birch, 1952), BMEOS3, and the fourth-order logarithmic equation of state (Poirier and Tarantola, 1998), LNEOS4, were fitted to the $E(V)$ data (Fig. 5). The zero pressure molar volumes, V_0, bulk moduli, K_0, first derivatives of the bulk modulus with respect to pressure, K_0', second derivatives of the bulk modulus with respect to pressure, K_0'', and energy per atom, E_0, resulting from this fitting procedure are given in Table 4. In addition, we have fitted four different equations of state directly to the external pressure output by VASP at the end of each volume relaxation (Fig. 6). The reason for doing this is that K_0 and K_0', are first and second derivatives of the pressure, but second and third derivatives of the total energy. Hence, we would expect that K_0', will be more accurately determined by fitting to the $P(V)$ results, and the magnitude of the standard errors on K_0', bear this out. The fitted equations are the third-order Birch–Murnaghan EOS, the fourth-order logarithmic EOS, the U2 "universal" EOS (Rose et al., 1984), and the Murnaghan Integrated Linear EOS, MILEOS (Murnaghan 1944). These parameters are also included in Table 4.

Within the errors due to fitting the EOS, both the monoclinic and orthorhombic cells have the same EOS. The arithmetic mean values of the EOS parameters in Table 4, with errors accommodating the maximum and minimum values of each parameter, are $V_0 = 52.748^{+0.122}_{-0.097}$ cm^{3}mol^{-1} ($350.37^{+0.81}_{-0.64}$ Å^3), $K_0 = 10.67^{+0.56}_{-0.44}$ GPA, and $K_0' = 5.38^{+2.52}_{-2.89}$.

No experimental data on the volume of ADH I as a function of pressure, $P(V)$, exist at present, so the EOS parameters presented here are to be considered as predictions that await future validation. However, our bulk modulus values fall between the calculated values for AMH I at

Table 3
Structural parameters for the ordered monoclinic unit cell of ADH I (variant A), derived from the disordered cubic cell (as described in Section II) and relaxed (as described in Section III)

Space group $P2_1$

a (Å) 7.0905
b (Å) 7.1870
c (Å) 7.1047
β 90.41°
V (Å^3) 362.04

Fractional atomic coordinates

	Wyckoff position	Occupancy	x	y	z
O1	2a	1	0.6567	0.6587	0.9117
H1	2a	1	0.2576	0.2408	0.0041
H2	2a	1	0.6652	0.5296	0.9643
O2	2a	1	0.1520	0.8449	0.5900
H3	2a	1	0.2343	0.7593	0.5076
H4	2a	1	0.0216	0.7914	0.5835
O3	2a	1	0.2017	0.1896	0.4426
H5	2a	1	0.7480	0.6704	0.6879
H6	2a	1	0.1782	0.0619	0.4946
O4	2a	1	0.6946	0.3054	0.0579
H7	2a	1	0.2503	0.8221	0.8127
H8	2a	1	0.4344	0.7503	0.9246
N1	2a	1	0.8761	0.8775	0.1264
H9	2a	1	0.9841	0.3614	0.9045
H10	2a	1	0.8589	0.8476	0.2662
H11	2a	1	0.1587	0.5145	0.8937
N2	2a	1	0.6279	0.1247	0.6216
H12	2a	1	0.5111	0.6445	0.4142
H13	2a	1	0.3556	0.6542	0.2384
H14	2a	1	0.6592	0.9871	0.6017

Note. The pattern of bond lengths is essentially the same as that given in Table 2 for the orthorhombic variant of ADH.

0 K (9.59 GPa, Fortes et al., 2001) and the extrapolated 0 K bulk modulus of Ice Ih (10.99 GPa, polynomial fit to data in Proctor 1966 and Dantl 1968). Our work on AMH I indicates that the temperature dependence of K_0 (dK_0/dT) from 0 to 100 K is ~0.006 GPa K^{-1}. This is virtually identical to the value for ice Ih over the same range derived from fitting to the data of Proctor (1966) and Dantl (1968), which yields $dK_0/dT = 0.0058$ GPa K^{-1}. Hence it is reasonable to assume a value of 0.006 GPa K^{-1} for dK_0/dT in ADH I from 0 to 100 K.

B. Thermal expansion

We can use our value for the zero pressure molar volume to make a further prediction regarding the thermal expansion of ADH I. Croft et al. (1988) adopted a thermal expansion coefficient derived for AMH, along with the single value for the lattice constant (at that time) of Bertie and Shehata (1984), to predict the density of ADH I at 0 K = 982.6(62) kg m^{-3}, or 54.00(39) cm^3 mol^{-1}. This value implies that our calculated zero pressure molar volume is too small by 2.3(9)%. In previous work we have found that the PW91 GGA functional compensates extremely well (while not properly representing dispersion forces) for the known deficiencies of the local density approximation (Hafner, 2000), such as overbinding, in solids whose structural strength is dominated by hydrogen-bonded water molecules (it leads to underbinding in ammonia-rich solids). For example, our calculated V_0 for AMH was within 0.3% of the 0 K value predicted by Croft et al. (1988), and just 1.6% smaller than the value derived by fitting an EOS to experimental $P(V)$ data at 115–150 K (see Fortes et al., 2001). We therefore consider it likely that ρ_0 for ADH estimated by Croft et al. (1988) is too low. The use of newly available neutron diffraction data (Loveday et al., 1999; Loveday and Nelmes, 1999, 2000), and other X-ray diffraction patterns (Durham et al., 1993), allows us to reassess this issue.

The lattice constant published by Bertie and Shehata (1984) at 105 K yields a density, ρ, of 977.3(62) kg m^{-3}. That of Loveday and Nelmes (2000) at 150 K yields ρ = 973.5(3) kg m^{-3} for *hydrogenous* ADH, using the lattice parameters of their *deuterated* structure. Moreover, we can use the ADH I powder pattern acquired at 170 K, and at 0.025 GPa, by Loveday et al. (1999) to calculate ρ. From the reflections 200, 201, 211, and 310, correcting for the applied

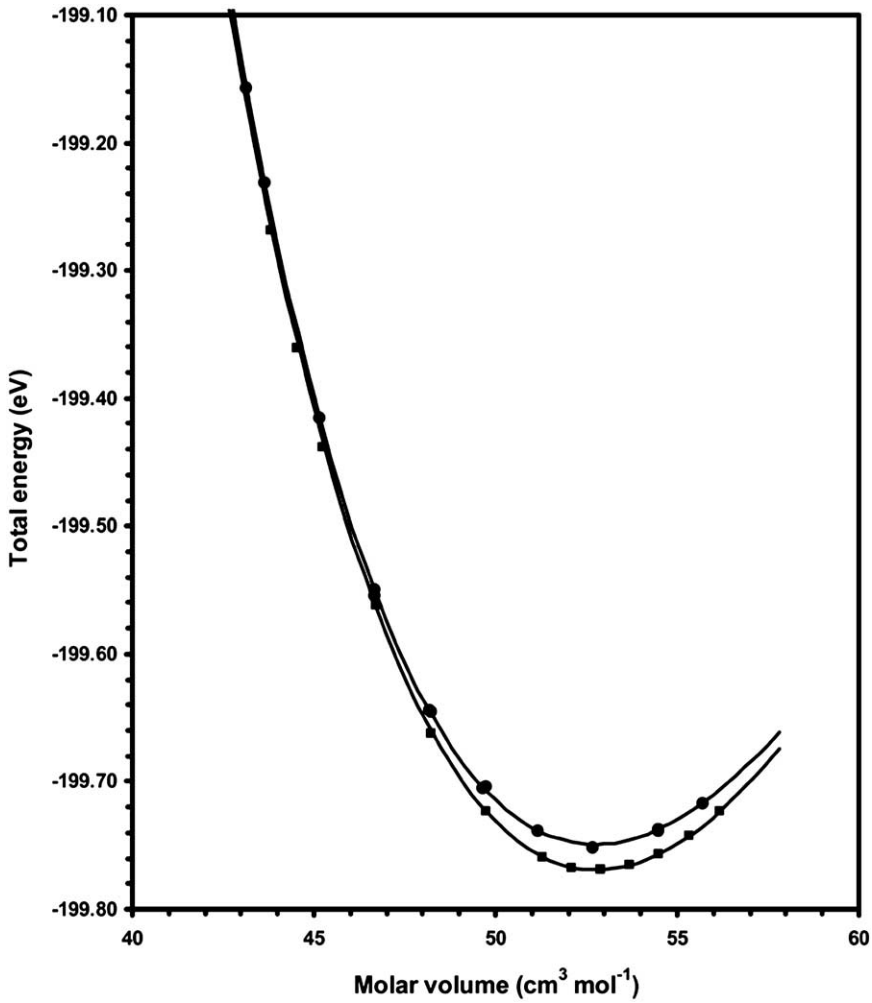

Fig. 5. Total energy per unit cell as a function of molar volume, *E(V)*, for the monoclinic ferroelectric cell (filled circles) and the orthorhombic antiferroelectric cell (filled squares). The solid lines are fourth-order logarithmic equations of state (EOS) fitted to the calculated *E(V)* values. The difference between the fourth- and third-order EOS are not visible at this scale.

pressure of 0.025 GPa using our calculated incompressibility, the density at 170 K is 966.1(16) kg m^{-3}. The large estimated error in this result is due to inaccuracies in measuring the *d*-spacings on the printed diffraction pattern.

Additional X-ray diffraction patterns appear in the paper of Durham et al. (1993). These patterns, acquired on mixed ice, AMH and ADH samples at 77 K (at 50 MPa) display Bragg peaks corresponding to $\{hkl\}$ = 110, 111, 200, 201, 211, 220, 310, and 311. The measured values of 2θ taken from these patterns, with the cell volume corrected for the pressure, yield a density for ADH I at 77 K of 970.7(85) kg m^{-3}. This is very much lower than expected, leading us to believe that the patterns might contain a systematic error. As a check, we also indexed the ice peaks and found an abnormally low density for ice at 77 K. The true density of ice at 77 K, calculated from the thermal expansion coefficient of

Table 4
Calculated equations of state (EOS) of the monoclinic and orthorhombic ADH cells

	Monoclinic-ADH I		Orthorhombic-ADH I		Fit to *combined* "external pressure" data for both structures			
	BMEOS3	LNEOS4	BMEOS3	LNEOS4	BMEOS3	LNEOS4	U2	MILEOS
V_0 (cm^3 mol^{-1})	52.724 (39)	52.745 (55)	52.837 (33)	52.756 (38)	52.730 (44)	52.712 (61)	52.718 (44)	52.763 (44)
K_0 (GPa)	10.56 (33)	10.75 (51)	10.75 (13)	11.01 (22)	10.58 (17)	10.57 (17)	10.57 (17)	10.59 (17)
K_0'	5.59 (39)	4.49 (200)	5.08 (16)	6.2 (17)	5.44 (19)	5.68 (58)	5.59 (18)	4.98 (15)
K_0'' (GPa^{-1})	—	1.4 (33)	—	−3.7 (5)	—	−1.1 (12)	—	—
E_0 (eV $molecule^{-1}$)	−49.937 (1)	−49.937 (1)	−49.9420 (2)	−49.9420 (2)	—	—	—	—

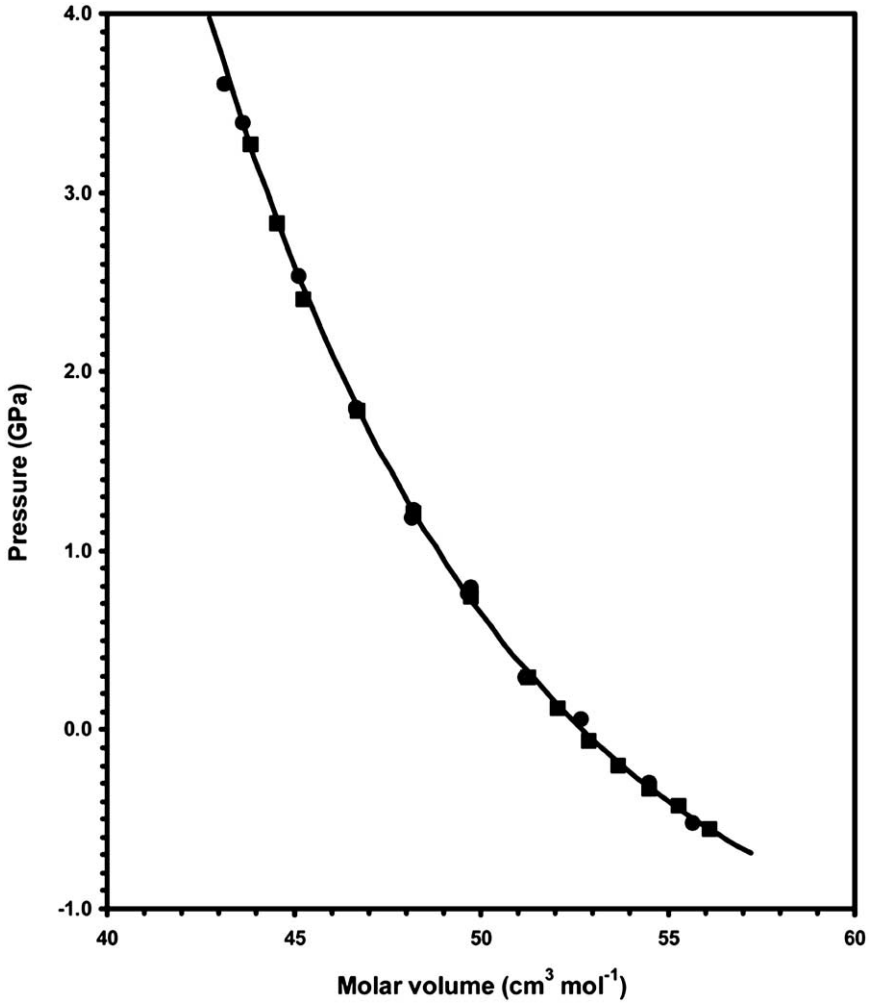

Fig. 6. The calculated external pressure as a function of molar volume, *P(V)*, for the monoclinic ferroelectric cell (filled circles) and the orthorhombic antiferroelectric cell (filled squares). The solid line is fourth-order logarithmic equations of state (EOS) fitted to the calculated *P(V)* values.

Croft et al. (1988) and also corrected for pressure, allowed us to amend this value of the density of ADH I. Finally, we used the liquid EOS of Croft et al. (1988), combined with the $\Delta V_{\text{melting}}$ from Hogenboom et al. (1997) of 1.03×10^{-6} m^3 mol^{-1}, to determine the density of the solid at the melting point. This appears on Fig. 7 as the open box. Fig. 7 shows the behavior of the density as a function of temperature.

Croft et al. (1988) employed a volume coefficient of thermal expansion, α_v, such that

$$\alpha_v = AT^B. \tag{1}$$

The density as a function of temperature at ambient pressure, $\rho(T)$, is thus

$$\rho(T) = \rho_0 \exp\left[-\left(\frac{A}{B+1}\right) T^{B+1} \right], \tag{2}$$

where ρ_0 is the density at absolute zero at ambient pressure, and A and B are empirical constants. Croft et al. (1988) adopted values of A and B derived for AMH: $A = 2.239 \times 10^{-7}$, and $B = 1.375$ (from 0 K to the melting point at 176.16 K), although it is worth observing that this fit was to just two data points. In the present study these three parameters were fitted to the density data by weighted nonlinear regression. The parameters A and B are not well constrained by the available data and so were fitted separately in order to yield physically sensible results. The resulting values are $\rho_0 = 991.7(39)$ kg m^{-3}, $A = 2.81(58) \times 10^{-7}$, and $B = 1.39(4)$. The value for ρ_0 is now just 1.4(6)% less than that obtained using V_0 from our equation of state, which is more in line with the modest degree of overbinding we have come to expect from calculations on ice-rich solids than the value of Croft et al. (1988). We believe that Fig. 7 depicts a more realistic prediction of $\rho(T)$ for ADH I.

The following subsection describes the calculated evolution of the cell shape as a function of pressure.

C. Elastic anisotropy

Fig. 8 shows that the incompressibilities (defined in the case of the *a* axis, for example, as $a^3 dP/da^3$) of the three cell edges

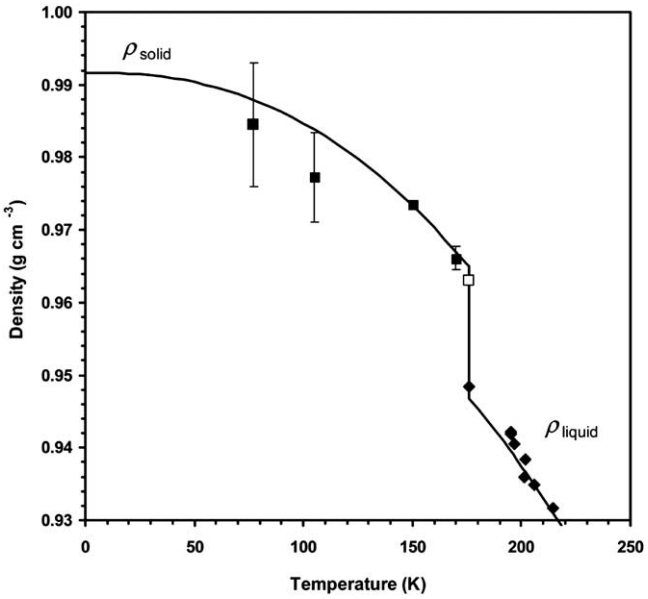

Fig. 7. Density of ammonia–water liquid and solid ADH at ambient pressure. The filled diamonds are the density measurements of Croft et al. (1988) on a solution containing ~29 wt% NH_3, and the line, ρ_{liquid}, passing through those points is the density of a 32.1 wt% NH_3 ammonia solution (corresponding to the stoichiometry of ADH) calculated using the EOS of Croft et al. (1988). The filled square at 105 K is from the X-ray diffraction experiment of Bertie and Shehata (1984). The filled square at 150 K is from the neutron diffraction experiment of Loveday and Nelmes (2000): Errors on that point are smaller than the symbol used. The filled square at 170 K shows the density derived from the unit cell dimensions we have calculated from a neutron diffraction pattern for ADH I, acquired at 170 K and 0.025 GPa by Loveday and Nelmes (1999), applying a correction for the modest pressure using the bulk modulus found in our ab initio simulations. The data point at 77 K was derived from the X-ray diffraction patterns of Durham et al. (1993). The line ρ_{solid} is based on the thermal expansion coefficient adopted for ammonia monohydrate by Croft et al. (1988). We have adjusted the empirical parameters to yield a better fit to the data, as described in the text.

are not the same. In this case (orthorhombic variant G), the *b* and *c* axes have linear incompressibilities of 9.6(10) and 9.4(19) GPa, respectively. The linear incompressibility of the *a* axis is 18(2.4) GPa. The monoclinic cell exhibits a similar pattern of axial incompressibilities. The reason for the difference becomes apparent when the arrangement of the water molecules along the crankshafts in each of the three directions (in variant G) is explicitly considered. Thus, the pattern along the crankshaft that is seen when looking down the *c* axis is O–H. . .O–H. . .O–H. . .O–H, etc., and the pattern seen when viewing down the *b* axis is the same, only reversed: O. . .H–O. . .H–O. . .H, etc. However, when looking down the *a* axis the pattern is subtly different: O–H. . .O. . . H–O–H. . .O. . .H–O–H, etc., and this is the cause of the differing axial incompressibilities.

V. Discussion

Chan and Giauque (1964) found that the entropy of ADH vanished in the low temperature limit, and concluded that the structure achieved full ordering of its hydrogen bonds at 0 K. Our results indicate that the lowest energy structure is antiferroelectrically ordered in orthorhombic space group $P2_12_12_1$. It is not possible, at absolute zero, for the disordered cubic cell to have a Gibbs free energy equal to, or lower, than the proposed orthorhombic cell because the disordered structure cannot be stabilized by entropy. It is physically impossible to disorder the orthorhombic cell without introducing defects into the structure, and since these defects require energy to form, the disordered unit cell must have a higher total energy.

There are then two possible ways in which the structure can behave over the temperature interval between absolute zero and its melting point at 176.16 K.

A. Model A

The heat capacity measurements (Fig. 9) of Chan and Giauque (1964) reveal no sign of a discontinuity that might be attributed to a sudden order–disorder transition, as in ammonia hemihydrate for example (Hildenbrand and Giauque, 1953). Perhaps, then, ADH I is fully ordered throughout its stability field. The diffraction patterns are readily explained by positing a domain model. It will be recalled from Section II that there are three orientational variants with 222 symmetry (which are related by threefold rotation axes). If ADH I were constructed from equal numbers of domains of each of these orthorhombic cells, and provided the domains were sufficiently small to diffract coherently and that the lattice strains are sufficiently small to allow a

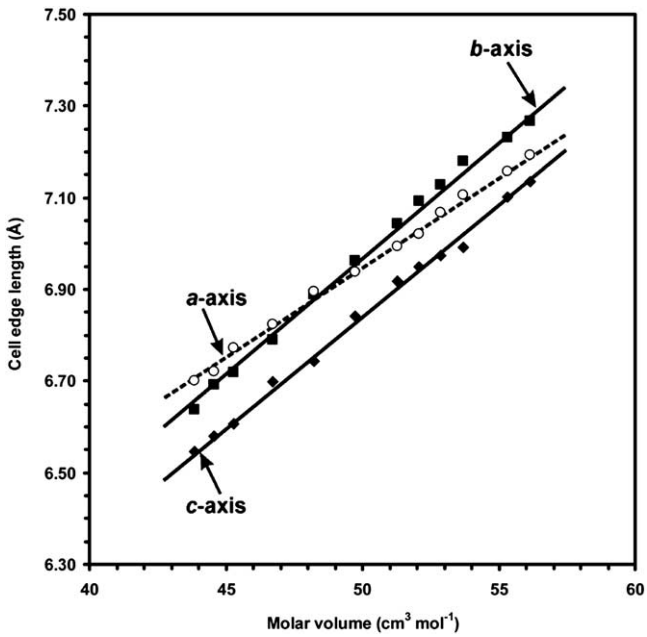

Fig. 8. Variation of the lattice parameters with volume in the orthorhombic cell (specifically, variant G: Fig 5). Circles, *a* axis; squares, *b* axis; diamonds, *c* axis. The *b* and *c* axes are significantly more compressible than the *a* axis. The monoclinic cell exhibits the same behavior.

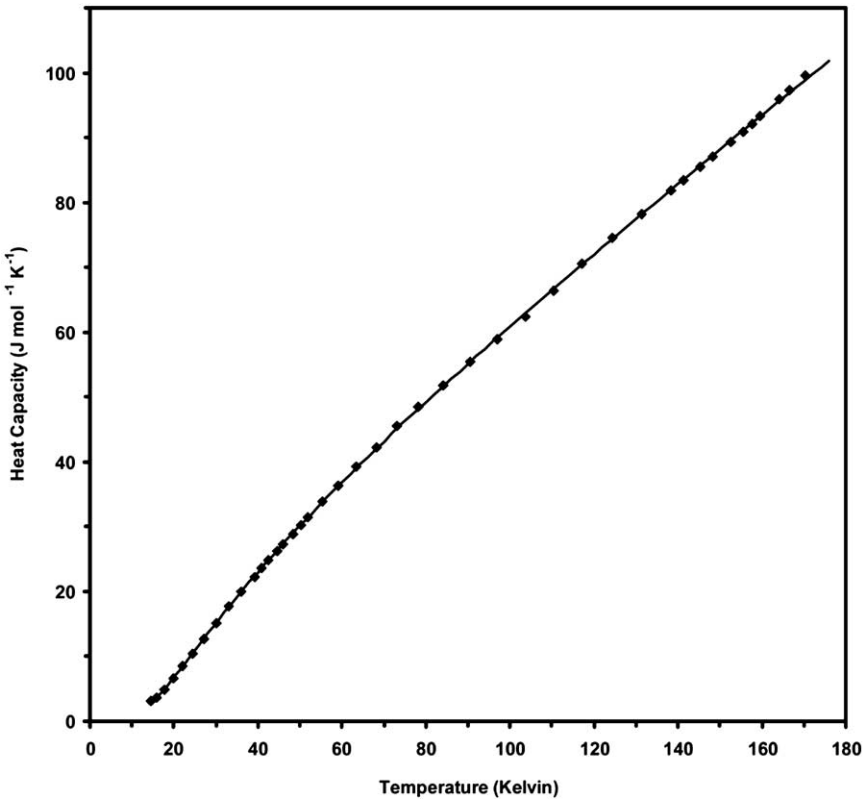

Fig. 9. The measured heat capacity, C_P, in NH_3.1.8687H_2O (33.59 wt% NH_3) and $NH_3 \cdot 1.9991H_2O$ (32.11 wt% NH_3) (after Chan and Giauque, 1964). The solid line is our best fit, of the form $C_P = a + bT + cT^{-2} + dT^{-1/2}$, where $a = 29.17(77)$, $b = 0.4862(27)$, $c = 2500(133)$, $d = -172(5)$: $R^2 = 99.996\%$. There is no evidence of a heat capacity anomaly that might be associated with an ordering of the water molecules at any temperature.

dimensionally cubic average lattice to be maintained throughout, the spatially averaged diffraction pattern would be cubic $P2_13$. It is straightforward to apply a threefold rotation matrix to the atomic coordinates of the orthorhombic cell so as to generate all of the virtual 1/3 and 2/3 occupied sites in the cubic cell.

Twinning (e.g., on the (020) plane) probably relates neighboring domains, and it is possible that rapid crystal growth will result in a microtwinned structure, whereas slow growth might yield a single domain crystal.

Although domain models per se have not enjoyed great success in explaining the structure of disordered minerals, the model described here can satisfy the experimental diffraction patterns, IR spectra, and heat capacity measurements.

B. Model B

The second possibility is that ADH I is not ordered throughout its stability field, but undergoes an order–disorder transition at some temperature at which the diffusion of orientational defects is still kinetically favored (i.e., above ~100 K). Model B may be summarized as follows: ADH I is paraelectrically disordered in space group $P2_13$ above the proposed transition temperature. Upon cooling, the water molecules fix themselves into preferred orientations, forming antiferroelectrically ordered domains. These ordered domains could nucleate in any one of three orthorhombic ($P2_12_12_1$) orientations, related by twin planes, resulting in either a macroscopically multiply twinned orthorhombic crystal or, in the limiting case of very fine-scale twinning, a structure equivalent to that of Model A. Model B is consistent with the IR spectra recorded at 100 K (Bertie and Shehata, 1984), and may be consistent with the heat capacity measurements if the transition occurs gradually; the change in entropy upon ordering will be very small, probably similar to that in water ice (~3 J mol^{-1}). The time-of-flight neutron diffraction experiments were at temperatures above the proposed transition temperature and so we would not expect to see evidence for peak splittings due to the formation of an orthorhombic microstructure. However, both of the X-ray diffraction experiments were at temperatures *below* the proposed transition temperature (105 K, Bertie and Shehata, 1984; 77K, Durham et al., 1993). We therefore estimate the extent of the likely peak splitting to determine whether it would have been resolvable. The largest orthorhombic strain at 0 K (along the *b* axis) is −0.89%. Along the *a* and *c* axes it is +0.46 and +0.43%, respectively. Hence, the maximum splitting at 0 K will be approximately 0.3° in 2θ at $2\theta = 40°$. At temperatures of 77–105 K this strain will be even smaller and the concomitant splitting is

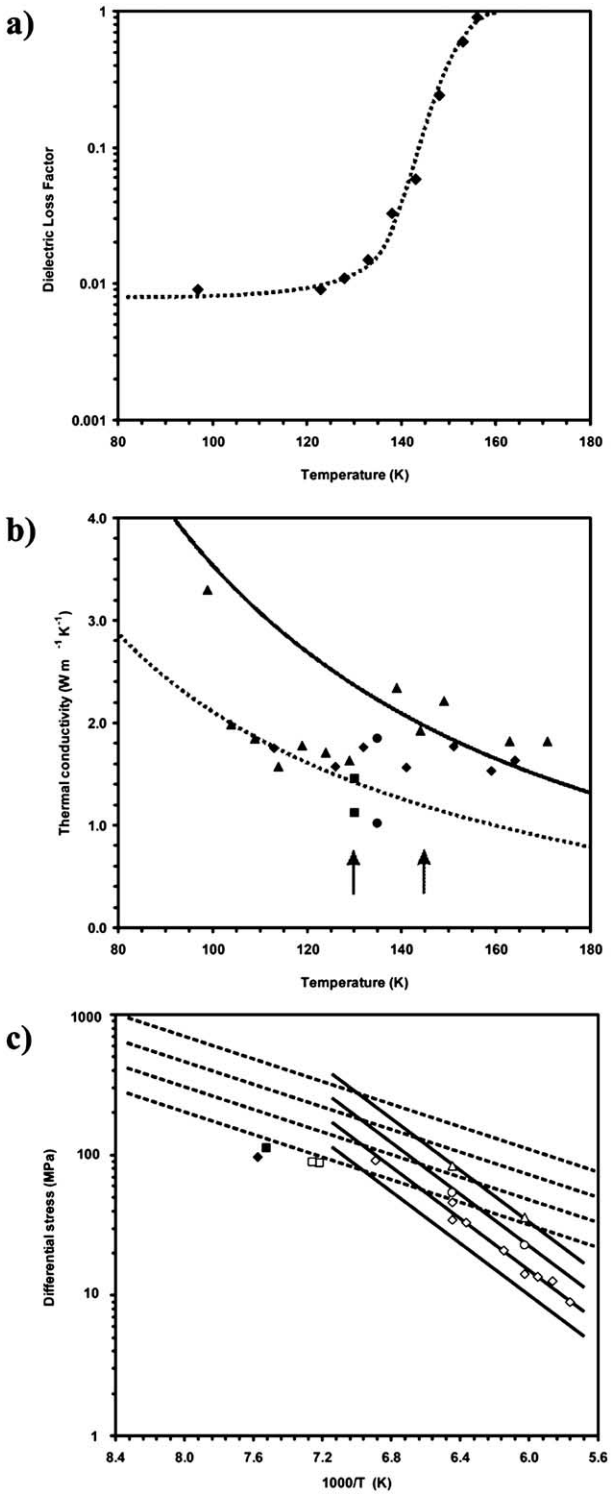

Fig. 10. (a) The dielectric loss factor (proportional to the loss tangent, tan $\delta = \varepsilon'/\varepsilon''$) for ice doped with 16 wt % NH_3 (i.e., 50:50 ice to ADH) measured at 2 kHz. Redrawn after Lorenz and Shandera (2001). The dotted line is a guide to the eye. (b) The thermal conductivity of ammonia-bearing ice (16 wt% NH_3, as above), redrawn after Lorenz and Shandera (2001). Triangles are hotwire results and diamonds are ammonia-rich samples after warming and refreezing. Circles are differentiated line source (Shandera and Lorenz, 2000) and squares are 30 wt% NH_3 from Kargel (1992). The solid black line is intended merely to indicate the expected behavior of $\lambda(T)$ and is based on the observed values for pure water ice. The dashed line shows the same temperature dependence but is lower by ~40%. Arrows bracket the proposed transition. (c) Arrhenius plot of the ductile strength of 29 wt% NH_3 ice (almost pure ADH, ideally) redrawn from Durham et al. (1993). The strain rates ($\dot{\varepsilon}$) are shown as triangles, $3.5 \times 10^{-4}\ s^{-1}$; circles, $3.5 \times 10^{-5}\ s^{-1}$; diamonds, $3.5 \times 10^{-6}\ s^{-1}$; boxes, $3.5 \times 10^{-7}\ s^{-1}$. Filled symbols show samples that failed and therefore represent a lower bound on the true strength. The derived flow laws at the specified strain rates for ADH are shown by solid black lines, and for water ice (after Durham et al., 1992) by dashed lines.

probably irresolvable in the patterns of Bertie and Shehata (1984) and Durham et al. (1993).

A gradual ordering transition also bears comparison with the behavior of a number of pure ice polymorphs: Upon cooling, ice III experiences a gradual proton ordering to become the isostructural (but antiferroelectrically ordered) phase ice IX (Whalley et al., 1968; Lobban et al., 2000). Similarly, ice V (space group $A2/a$) undergoes a gradual transformation to an antiferroelectrically ordered structure (space group $P2_1/a$), although the latter is unstable with respect to ice II (Kamb and La Placa, 1974; Lobban et al., 2000; Johari and Whalley, 2001).

However, we would expect significant changes in other experimentally observable quantities if ADH I undergoes an order–disorder transition, and so we now review literature evidence in support of Model B.

Experimental evidence for an order–disorder transition

There appears to be a very dramatic change in the dielectric behavior (Lorenz, 1998; Lorenz and Shandera, 2001), the thermal conductivity as a function of temperature, $\lambda(T)$ (Lorenz and Shandera, 2001), and in the creep behavior (Durham et al., 1993) of ammonia-bearing ices in the temperature interval 130–150 K (Fig. 10). The changes in the creep and dielectric behavior are consistent with ADH being wholly or partially disordered above 150 K and fully ordered from 130 K down to absolute zero. The meaning of the change in the thermal conductivity is not clear.

The dielectric properties are the most leading piece of evidence because of the way that water molecules in ice respond to an applied a.c. electric field. In the dynamically disordered ice phases, reorientation of the water molecules (due to Bjerrum defect diffusion) results in a larger contribution to the dielectric permittivity from orientational polarization at lower frequencies. In the fully ordered phases (e.g., ice II), this orientational polarization is absent, since the water molecules are fixed in place, and the high-frequency dielectric permittivity (ε_∞) is the same as the low-frequency dielectric permittivity (ε_0). Analysis of this dielectric dispersion is a powerful means of probing the degree of orientational order in ice crystals. The dielectric study of the ice III ↔ ice IX transition is an excellent example (Whalley et al., 1968), as is the recent study of partial ordering in ice V (Johari and Whalley, 2001).

The temperature-dependent complex permittivity measurements of Lorenz and Shandera (2001) show a very

dramatic change in the dielectric properties of ice doped with ammonia between 130 and 150 K (Fig. 10a). The sample in question consisted of ice doped with 16 wt% NH_3 (i.e., ~50% water ice, 50% ADH). It is probable that there was a finite quantity of metastable AMH in the sample but since AMH I is fully ordered our conclusion is unaffected. The observed change is characterized by a drop in the loss tangent, tan(δ) (the ratio of the real, ε', to the imaginary part, ε'', of the complex dielectric constant, $\varepsilon_0 = \varepsilon' + i\varepsilon''$) upon cooling. This can only be attributed to a reduction of the orientational polarization contribution from the water molecules in the sample. However, the reorientation of the water molecules in ice becomes frozen in at temperatures of ~100 K, and so the observed dielectric signature must be due to ordering of the water molecules in ADH I. Ice doped with 5 wt% NH_3 exhibits the same behavior.

The measured thermal conductivity as a function of temperature, $\lambda(T)$, is shown in Fig. 10b (after Lorenz and Shandera, 2001). Above 140 K, the data are well fitted by a function that varies in the same fashion as in ice Ih. The solid black line depicts a temperature dependence based on that of ice (e.g., Andersson and Suga, 1994); $\lambda(T) = (500/T) - 1.45$. Below 140 K λ appears to be anomalously low. The dotted curve shows the same temperature dependence as the black line but is systematically offset to lower values by ~40%. At the order–disorder transition in hexagonal ice (ice Ih ↔ ice XI) proton ordering is believed to decrease the lattice anharmonicity, producing an increase in λ of ~20% at the transition (Andersson and Suga, 1994). Invoking a similar mechanism for the ordering transition in ADH, we would therefore expect λ to rise at 140 K rather than dropping. Hence, the thermal conductivity data can be interpreted as showing a change in transport properties near 140 K, but this change is in the opposite sense to that seen through the orientational ordering transition from ice Ih to ice XI.

The creep of ices in the ammonia–water system was studied by Durham et al. (1993). Their work revealed that ADH is four orders of magnitude less viscous than pure water ice at temperatures just below its melting point, but exhibits a steeper temperature dependence. This results in ADH becoming as viscous as water ice at ~140 K. Similar mechanical behavior was observed by Lorenz and Shandera (2001). However, the temperature dependence appears to change below 140 K. Fig. 10c shows the data for 29 wt% NH_3 (ideally 90% ADH, 10% ice) samples at four strain rates. Solid black lines depict the flow law for this composition as derived from the data points (Durham et al., 1993). The dotted lines depict the flow law for pure water ice at the same strain rates (after Durham et al., 1992). Note that, below 140 K ($1000/T = 7.15$), the strength of the ADH samples lies below the extension of the flow law fitted to the higher temperature measurements. Durham et al. (1993) believe that the dominant flow mechanism in ADH changes below 145 K. In ice, creep is dominated by basal slip, which is assisted by the migration of orientational defects. We would therefore argue that the observed softening of ADH above 140 K is due to the appearance of rotational defects as the water molecules become disordered.

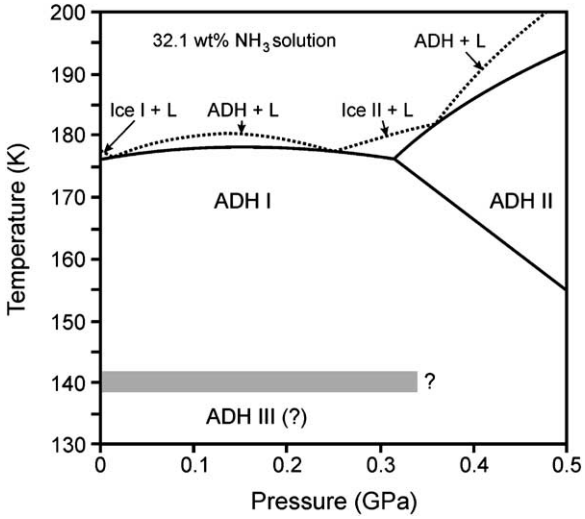

Fig. 11. Pseudo-unary phase diagram for ADH in *P–T* space, adapted after Hogenboom et al. (1997) with corrections to depict the probable shape of the liquidus surface. The complex liquidus is due to the repeated shift from incongruent to congruent melting that occurs at higher pressures. ADH melts incongruently to an ice polymorph + ammonia-rich fluid (xNH$_3$ > 32.1wt%), or it melts congruently to ADH + water-rich fluid (xNH$_3$ < 32.1wt%).

The experimental evidence outlined above therefore appears to indicate that there is a transition from wholly or partially disordered ADH I to a fully ordered phase, which we provisionally call ADH III. By analogy with order–disorder transitions in ice polymorphs, the volume change upon ordering is likely to be negligible (e.g., Suga, 1997). Hence the phase boundary between ADH I and ADH III will have $dT/dP \sim 0$, and the probable phase diagram will be as depicted in Fig. 11.

The model requires rigorous testing; most useful would be dielectric spectroscopy at a range of temperatures, careful measurements of the heat capacity of both rapidly cooled (and unannealed) samples and annealed samples (see Johari, 2000), and high-resolution X-ray or neutron diffraction studies as a function of temperature. Care should also be taken with the sample preparation technique since the behavior of ADH may depend on whether the sample is grown slowly from the liquid phase (at pressures where ADH I melts congruently; i.e., ~15–240 MPa) or flash cooled into a glass and then annealed, the latter being the method of choice for most of the experimental work referenced herein.

VI. Implications

The EOS data that we have presented allow us to calculate the density of ADH I under *P–T* conditions relevant to the interiors of many icy moons. Thus we can develop

structural and thermal models of icy moons containing ADH I. Although Titan is widely cited, as indeed it is here, as the archetypal ammonia-bearing icy moon, it is unlikely that there are substantial quantities of crystalline ADH I in Titan's interior. In order to crystallize ADH I in Titan's interior, temperatures in the upper mantle (i.e., the topmost few hundred kilometers) would need to be below 176 K. The thermal structure models of Grasset et al. (2000) indicate that this is highly improbable, upper mantle temperatures being ~200–220 K. Hence Titan could have an ammonia–water aquasphere some 200–400 km deep under a crust of ice but no ADH I. ADH I may be present if NH_3–H_2O fluids can permeate the crust, and so our EOS may have use in determining the relative densities of liquids and solids in cooling cryomagmatic systems (e.g., plutons). Furthermore, ADH I could have been stable in the uppermost few hundred kilometers of Titan's primitive mantle prior to differentiation.

However, there are many smaller icy moons around Saturn and Uranus wherein the *P–T* conditions do favor the crystallization of ADH I. Saturn's second largest moon Rhea, for example, is small enough, and probably cold enough, to allow for an extensive layer of ADH I to be present in its interior. Although we are developing more comprehensive structural and thermal models of the saturnian and uranian moons, our initial work indicates that ADH I will, assuming $x\mathrm{NH}_3 = 15$ wt%, form a layer ~255 km thick (at *T* from 90 to 110 K, and *P* from ~35 to 100 MPa) between a 140-km-thick crust of ice Ih and a rocky core ~740 km in diameter inside Rhea. This model is consistent with the observed radius and density of Rhea, and yields values for the moment of inertia, quadrupole gravitational moments, and triaxial figure for comparison with future *Cassini* observations.

The crystallization of a eutectic ammonia–water aquasphere into ADH I inside the saturnian and uranian moons may well be the explanation for the observed rifting and cryovolcanic resurfacing seen on these moons. Consolmagno (1985) modeled the global thermal expansion of the saturnian satellites resulting from solidification of an ammonia–water aquasphere. He concluded that that the uncertainties in bulk modulus and thermal expansivity needed to be better than 1% in order to determine whether the freezing of an eutectic fluid could explain the observed geology. We are confidant that our EOS is sufficiently accurate to do this, and so we are at present reevaluating the Consolmagno model of thermal expansion, not only for the moons of Saturn, but for the moons of Uranus as well.

Since ADH I in these small icy bodies is typically likely to be present at temperatures below the proposed ordering temperature, it seems clear that there is a need to extend experimental studies on properties such as thermal conductivity, dielectric permittivity, and viscosity (amongst others) to these low temperatures. Our model offers a microscopic explanation for changes in the strength and transport properties of ADH suggested by the experiments cited in Section V. Changes in strength and thermal conductivity will influence the thermal evolution of the whole satellites, and differences in dielectric properties may affect the way that surface deposits of ADH reflect radio waves from the *Cassini* radar instrument.

VII. Summary

We have determined that there are only two possible ordering schemes for the water molecules in phase I of ammonia dihydrate that satisfy the ice rules. One is ferroelectrically ordered in space group $P2_1$. The other is antiferroelectrically ordered in space group $P2_12_12_1$. Our ab initio calculations show that the latter is more energetically stable by 5 meV per formula unit (~0.5 kJ mol^{-1}). The calculated energy–volume curves of the ordered cells have been fitted to several equations of state, yielding mean values for the EOS parameters of $V_0 = 52.748^{+0.122}_{-0.097}$ $\mathrm{cm}^3\mathrm{mol}^{-1}$, $K_0 = 10.67^{+0.56}_{-0.44}$ GPa, and $K_0' = 5.38^{+2.52}_{-2.89}$. In addition, we have reassessed the coefficient of volume thermal expansion using recent literature data. The incompressibility of the *a* axis is found to be significantly greater than that along the *b* or *c* axes.

We believe that the experimental observations show evidence for a gradual order–disorder transition between 130 and 150 K. Above this temperature, ADH I is paraelectrically disordered. Upon cooling to 150 K, antiferroelectrically ordered domains nucleate and grow until the entire structure is ordered below 130 K. We call this possible ordered low-temperature phase ADH III.

Further investigations, in particular of the dielectric properties as a function of temperature, are warranted to establish the degree of ordering in ADH.

Acknowledgments

A.D.F. acknowledges a scholarship from the UCL Graduate School in support of this work. L.V. and J.P.B. acknowledge a Royal Society Fellowship. The authors thank David Price, Stephen K. Croft, and two anonymous referees for useful comments.

References

Andersson, O., Suga, H., 1994. Thermal conductivity of the Ih and XI phases of ice. Phys. Rev. B 50, 6583–6588.

Andrews, S.B., Burton, N.A., Hillier, I.H., 1997. A corrective potential for hydrogen in density functional calculations. Chem. Phys. Lett. 280, 73–78.

Bernal, J.D., Fowler, R.H., 1933. A theory of water and ionic solutions, with particular reference to hydrogen and hydroxyl ions. J. Chem. Phys. 1, 515–548.

Bertie, J.E., Shehata, M.R., 1984. Ammonia dihydrate: preparation, X-ray powder diffraction pattern and infrared spectrum of $NH_3 \cdot 2H_2O$ at 100K. J. Chem. Phys. 81, 27–30.

Birch, F., 1952. Elasticity and constitution of the Earth's interior. J. Geophys. Res. 57, 227–286.

Bjerrum, N., 1951. Structure and properties of ice I. The position of hydrogen atoms and the zero-point entropy of ice. Kgl. Danske. Videnskab. Selskab. Math. Fys. Medd. 27 (1), 3–56.

Bjerrum, N., 1952. Structure and properties of ice. Science 115, 385–390.

Chan, J.P., Giauque, W.F., 1964. The entropy of $NH_3 \cdot 2H_2O$. Heat capacity from 15 to 300°K. J. Phys. Chem. 68, 3053–3057.

Consolmagno, G.J., 1985. Resurfacing of Saturn's satellites: models of partial differentiation and expansion. Icarus 64, 401–413.

Croft, S.K., Lunine, J.I., Kargel, J.S., 1988. Equation of state of ammonia-water liquid: derivation and planetological implications. Icarus 73, 279–293.

Dantl, G., 1968. Die elastischen moduln von eis-einkristallen. Phys. Condens. Matter 7, 390–397.

Demaison, J., Margulès, L., Boggs, J.E., 2000. The equilibrium N-H bond length. Chem. Phys. 260, 65–81.

Durham, W.B., Kirby, S.H., Stern, L.A., 1992. Effects of dispersed particulates on the rheology of water ice at planetary conditions. J. Geophys. Res. 97, 20883–20897.

Durham, W.B., Kirby, S.H., Stern, L.A., 1993. Flow of ices in the ammonia-water system. J. Geophys. Res. 98, 17667–17682.

Fortes, A.D., 2000. Exobiological implications of a possible ammonia-water ocean inside Titan. Icarus 146, 444–452.

Fortes, A.D., Brodholt, J.P., Wood, I.G., Vočadlo, L., Jenkins, H.D.B., 2001. Ab initio simulation of ammonia monohydrate ($NH_3 \cdot H_2O$) and ammonium hydroxide (NH_4OH). J. Chem. Phys. 115, 7006–7114.

Gränicher, H., 1958. Lattice disorder and physical properties connected with the hydrogen arrangement in ice crystals. Proc. R. Soc. London A 247, 453–461.

Grasset, O., Sotin, C., 1996. The cooling rate of a liquid shell in Titan's interior. Icarus 123, 101–123.

Grasset, O., Sotin, C., Deschamps, F., 2000. On the internal structure and dynamics of Titan. Planet. Space. Sci. 48, 617–636.

Hafner, J., 2000. Atomic-scale computational materials science. Acta Mater. 48, 71–92.

Hamann, D.R., 1997. H_2O hydrogen bonding in density functional theory. Phys. Rev. B 55, 10157–10160.

Hildenbrand, D.L., Giauque, W.F., 1953. Ammonium oxide and ammonium hydroxide. Heat capacities and thermodynamic properties from 15 to 300°K. J. Am. Chem. Soc. 75, 2811–2818.

Hogenboom, D.L., Kargel, J.S., Consolmagno, G.J., Holden, T.C., Lee, L., Buyyounouski, M., 1997. The ammonia-water system and the chemical differentiation of icy satellites. Icarus 128, 171–180.

Hohenberg, P., Kohn, W., 1964. Inhomogenous electron gas. Phys. Rev. B 136, B864–B871.

Jensen, P., 1989. The potential-energy surface for the electronic ground-state of the water molecule determined from experimental-data using a variational approach. J. Mol. Spectrosc. 133, 438–460.

Johari, G.P., 2000. On the origin of the heat capacity feature of annealed ices and ice clathrates, and interpreting water's diffusivity in terms of the entropy. Chem. Phys. 258, 277–290.

Johari, G.P., Whalley, E., 2001. The dielectric relaxation time of ice V, its partial anti-ferroelectric ordering and the role of Bjerrum defects. J. Chem. Phys. 115, 3274–3280.

Johnson, M.L., Nicol, M., 1987. The ammonia-water phase diagram and its implications for icy satellites. J. Geophys. Res. 92, 6339–6349.

Kamb, B., La Placa, S.J., 1974. Reversible order-disorder transformation in ice V. Eos. Trans. Am. Geophys. Union 55, 1202.

Kargel, J.S., 1992. Ammonia-water volcanism on icy satellites: phase relations at 1 atmosphere. Icarus 100, 556–574.

Kohn, W., Sham, L.J., 1965. Self-consistent equations including exchange and correlation effects. Phys. Rev. B 140, A1133–A1138.

Kresse, G., Furthmüller, J., 1996. Efficient iterative schemes for ab initio total-energy calculations using a plane wave basis set. Phys. Rev. B 54, 11169–11186.

Lewis, J.S., 1972. Low temperature condensation from the solar nebula. Icarus 16, 241–252.

Lobban, C., Finney, J.L., Kuhs, W.F., 2000. The structure and ordering of ices III and V. J. Chem. Phys. 112, 7169–7180.

Lorenz, R.D., 1998. Preliminary measurements of the cryogenic dielectric properties of water-ammonia ices: Implication for radar observations of icy satellites. Icarus 136, 344–348.

Lorenz, R.D., Shandera, S.E., 2001. Physical properties of ammonia-rich ice: application to Titan. Geophys. Res. Lett. 28, 215–218.

Loveday, J.S. and Nelmes R.J. 1999. The ambient pressure structure of ammonia dihydrate. ISIS Facility Experimental Report (POLARIS) RB 9411a. Rutherford Appleton Laboratory, RAL-TR-1999-050.

Loveday, J., Nelmes, R.J., 2000. Structural studies of ammonia hydrates, in: Manghnani, M.H., Nellis, W.J., Nicol, M.T. (Eds.), Science and Technology of High Pressure: Proceedings of AIRAPT-17, Universities Press, Hyderabad, India, pp. 133–136.

Loveday, J.S. Guthrie, M. and Nelmes, R.J. 1999. Structural changes under pressure in ammonia dihydrate and ammonia hemihydrate. ISIS Facility Experimental Report (POLARIS) RB 9859. Rutherford Appleton Laboratory, RAL-TR-1999-050.

Lunine, J.I., Yung, Y.L., Lorenz, R.D., 1999. On the volatile inventory of Titan from isotopic abundances in nitrogen and methane. Planet. Space. Sci. 47, 1291–1303.

Monkhorst, H.J., Pack, J.D., 1976. Special points for Brillouin-zone integrations. Phys. Rev. B 13, 5188–5192.

Murnaghan, F.D., 1944. The compressibility of media under extreme pressures. Proc. Natl. Acad. Sci. USA 30, 244–247.

Perdew, J.P., Wang, Y., 1992. Accurate and simple representation of the electron-gas correlation energy. Phys. Rev. B 45, 13244–13249.

Podeszwa, R., Buch, V., 1999. Structure and dynamics of orientational defects in ice. Phys. Rev. Lett. 83, 4570–4573.

Poirier, J.-P., Tarantola, A., 1998. A logarithmic equation of state. Phys. Earth. Planet. Int. 109, 1–8.

Prinn, R.G., Fegley, B., 1981. Kinetic inhibition of CO and N_2 reduction in circumplanetary nebulae-implications for satellite composition. Astrophys. J. 249, 308–317.

Proctor, T.M., 1966. Low temperature speed of sound in single-crystal ice. J. Acoust. Soc. Am. 39, 972–977.

Rose, J.H., Smith, J.R., Guinea, F., Ferrante, J., 1984. Universal features of the equation of state of metals. Phys. Rev. B 29, 2963–2969.

Shandera, S., and Lorenz R. 2000. Thermal conductivity and microwave absorptivity of ammonia hydrate ice. Lunar Planet. Sci. XXXI, CD-ROM abstract 1485.

Stevenson, D.J., 1982. Volcanism and igneous processes in small icy satellites. Nature 298, 142–144.

Suga, H., 1997. A facet of recent ice sciences. Thermochim. Acta 300, 117–126.

Tsuzuki, S., Lüthi, H.P., 2001. Interaction energies of van der Waals and hydrogen bonded systems calculated using density functional theory: assessing the PW91 model. J. Chem. Phys. 114, 3949–3957.

Vanderbilt, D., 1990. Soft self-consistent pseudopotentials in a generalized eigenvalue problem. Phys. Rev. B 41, 7892–7895.

Whalley, E., Heath, J.B.R., Davidson, D.W., 1968. Ice IX: an antiferroelectric phase related to ice III. J. Chem. Phys. 48, 2362–2370.

Yarger, J., Lunine, J.I., Burke, M., 1993. Calorimetric studies of the ammonia-water system with application to the outer Solar System. J. Geophys. Res. 98, 13109–13117.